LSTM- GA Enhanced Power Quality Improvement in STATCOM Integrated SPV Microgrid

Durgamadhab Swain¹, Meera Viswavandya²

¹Research Scholar, Department of Electrical Engineering, Biju Patnaik University of Technology, Rourkela India; Department of Electrical Engineering, Ajay Binay Institute of Technology, Cuttack 753014, India ²Department of Electrical Engineering, Odisha University of Technology and Research, Bhubaneswar, India

Abstract:-This research explores the performance of various control techniques for Static Synchronous Compensators (STATCOM) and Doubly Fed Induction Generators (DFIG) in microgrid environments, with a focus on the integration of solar photovoltaic (SPV) systems. The study compares Fuzzy Proportional-Integral (Fuzzy-PI), Particle Swarm Optimization-tuned PI (PSO-PI), and Long Short-Term Memory-Genetic Algorithm optimized PI (LSTM-GA-PI) controllers, analyzing their impact on time-domain response, harmonic distortion, and power quality. Incorporating SPV systems into microgrids facilitates the use of renewable energy, reducing dependence on fossil fuels and lowering greenhouse gas emissions, thus enhancing environmental sustainability. The coordinated control between SPV and STATCOM improves power quality by ensuring stable voltage and frequency, optimizing energy use, and reducing electrical disturbances and waste. The results show that the LSTM-GA-PI controller outperforms the other methods, achieving the fastest response times and the lowest maximum overshoot, while also significantly reducing Total Harmonic Distortion (THD) in both voltage and current. This underscores the LSTM-GA-PI controller's capability to enhance microgrid performance by maintaining stable and efficient power quality. Advanced control techniques like LSTM and GA enable microgrids to adapt to changing conditions, minimize losses, and improve energy flow. This study demonstrates that integrating these algorithms into STATCOM and SPV systems provides a robust solution for achieving high stability and power quality in diverse operational scenarios, promoting more reliable and efficient microgrid implementations.

Keywords: LSTM, GA, STATCOM, SPV, Microgrid

1. Introduction

Microgrids have emerged as a crucial component in the modern energy landscape, offering a sustainable and resilient solution to the growing demand for reliable power. These localized energy systems can operate independently or in conjunction with the main grid, providing flexibility and enhancing the stability of the overall power network. By integrating renewable energy sources such as solar photovoltaic (SPV) systems, microgrids significantly reduce dependence on fossil fuels, lowering greenhouse gas emissions and promoting environmental sustainability [1][2]. The advanced control mechanisms employed within microgrids, including coordination between SPV and STATCOM, ensure consistent power quality, stable voltage, and frequency levels. Additionally, innovative techniques like Long Short-Term Memory (LSTM) and Genetic Algorithms further optimize performance, enabling microgrids to adapt to changing conditions, minimize energy losses, and maximize the utilization of renewable resources. As a result, microgrids not only contribute to a more efficient and eco-friendly energy system but also enhance resilience against natural disasters and other disruptions, ensuring a reliable and uninterrupted power supply [3][4].

AC-DC microgrids represent a significant advancement in the field of energy distribution, combining the advantages of both alternating current (AC) and direct current (DC) systems [5]. This hybrid approach offers superior flexibility, efficiency, and reliability compared to traditional AC-only or DC-only microgrids. By integrating AC and DC sources, AC-DC microgrids can efficiently manage a diverse range of energy resources,

including solar photovoltaic (SPV) systems, batteries, and conventional generators [6]. This dual capability allows for optimal energy conversion and distribution, minimizing losses and enhancing overall system performance [7].

One of the primary benefits of AC-DC microgrids is their ability to accommodate the increasing prevalence of renewable energy sources, which often generate DC power. By directly incorporating these sources into the grid without the need for multiple conversions, AC-DC microgrids improve energy efficiency and reduce operational costs [8][9]. Additionally, the integration of advanced control techniques ensures stable and consistent voltage and frequency levels, contributing to improved power quality and reliability [10].

The control of microgrids presents several critical challenges that must be addressed to fully harness their potential for providing reliable, sustainable, and efficient energy. Microgrids, which can operate independently or in conjunction with the main grid, integrate a variety of energy sources, including renewables like solar photovoltaic (SPV) systems and conventional generators. This diversity necessitates sophisticated control mechanisms to manage the coordination between different power sources and ensure stable and consistent voltage and frequency levels [11][12].

One of the primary issues in microgrid control is maintaining power quality amidst the variable nature of renewable energy sources. Fluctuations in energy production can lead to voltage sags, swells, and frequency deviations, which can disrupt the stability of the grid. Effective coordination between SPV systems and devices such as Static Synchronous Compensators (STATCOM) is essential to mitigate these issues, ensuring a smooth and reliable power supply. Another significant challenge is optimizing energy consumption and minimizing losses. Advanced control techniques, such as those utilizing machine learning algorithms like Long Short-Term Memory (LSTM) and Genetic Algorithms, are required to dynamically adjust to changing conditions and optimize the energy flow. These intelligent systems can enhance the overall efficiency and performance of the microgrid, making it more resilient and adaptive [13].

2. Objectives

The primary objective of this research is to design and implement a Static Synchronous Compensator (STATCOM) specifically for microgrid environments, focusing on providing reliable voltage and reactive power support under varying environmental conditions. Microgrids, which consist of distributed energy resources like solar panels and wind turbines, often face significant challenges in maintaining power quality due to fluctuations in energy output. Voltage sags, swells, and harmonic distortions are common issues that can adversely impact the stability and reliability of these systems. To address these challenges, the researchers propose an advanced control strategy that integrates Long Short-Term Memory (LSTM) networks with Genetic Algorithms (GA) to optimize the performance of STATCOMs, thereby ensuring efficient and effective power quality management [14].

The innovative LSTM-GA model developed in this research leverages the strengths of both machine learning and evolutionary algorithms. LSTM networks, known for their ability to retain and analyze historical data, are employed to store and process past power quality issues and reactive power support requirements. This historical data is crucial for predicting and managing future disturbances in the microgrid. Meanwhile, the GA component is used to optimize the hyperparameters of the control system, which includes tuning the STATCOM's operational parameters for optimal performance. This combined approach not only accelerates the process of identifying the best control parameters but also reduces the computational complexity typically associated with grid searches or manual tuning, making the system more efficient and reliable [15][16].

To achieve the research objectives, comprehensive modeling and simulation of the STATCOM are conducted using MATLAB Simulink. This simulation framework allows for a detailed analysis of the STATCOM's performance under various dynamic non-linear loading conditions and environmental variations. By simulating different scenarios, the researchers can evaluate how the STATCOM responds to real-time changes in the microgrid, such as fluctuations in renewable energy output or sudden changes in load demand. The LSTM component of the model processes the input data to provide reactive power support, while the GA component continuously optimizes the control parameters to enhance performance. This meticulous simulation and validation

process is critical in demonstrating the effectiveness of the proposed LSTM-GA control strategy in real-world applications [17].

3. Methods

The SIMB (Smart Integrated Microgrid and Building) architecture diagram as presented at fig.1 illustrates a comprehensive setup for a microgrid system that integrates multiple sources of energy generation and critical loads. Starting from the left, the grid supplies the primary power, which is first stepped down by Transformer 1 (TRF-1). This power is then distributed to various components in the microgrid. The Micro Hydro Turbine (MHT) connects to the main power line after TRF-1, contributing additional renewable energy. Below the main line, an EV Charging station is connected to facilitate the charging of electric vehicles, indicating a focus on sustainable and renewable energy integration within the microgrid.

In the central part of the diagram, two critical loads are represented. Critical Load-1 is connected via a secondary line and is associated with Photovoltaic (PV) panels, which provide solar power to the microgrid. This setup emphasizes the use of renewable energy sources within the system. Critical Load-2, on the other hand, is connected directly to the main power line after the MHT, showing the system's capability to support essential loads with multiple sources of energy. This part of the diagram highlights the flexibility and resilience of the microgrid in maintaining power supply to critical infrastructures.

Towards the right end of the diagram, Transformer 2 (TRF-2) steps down the voltage once more, leading to a Voltage Source Converter (VSC) that is responsible for converting power to suitable forms for specific applications. Connected to the VSC is the Control Logic, which manages the operations and control within the microgrid, ensuring efficient and reliable power distribution. An optional Energy Storage component is also shown, which can store excess energy generated by the microgrid for later use, enhancing the system's efficiency and reliability..

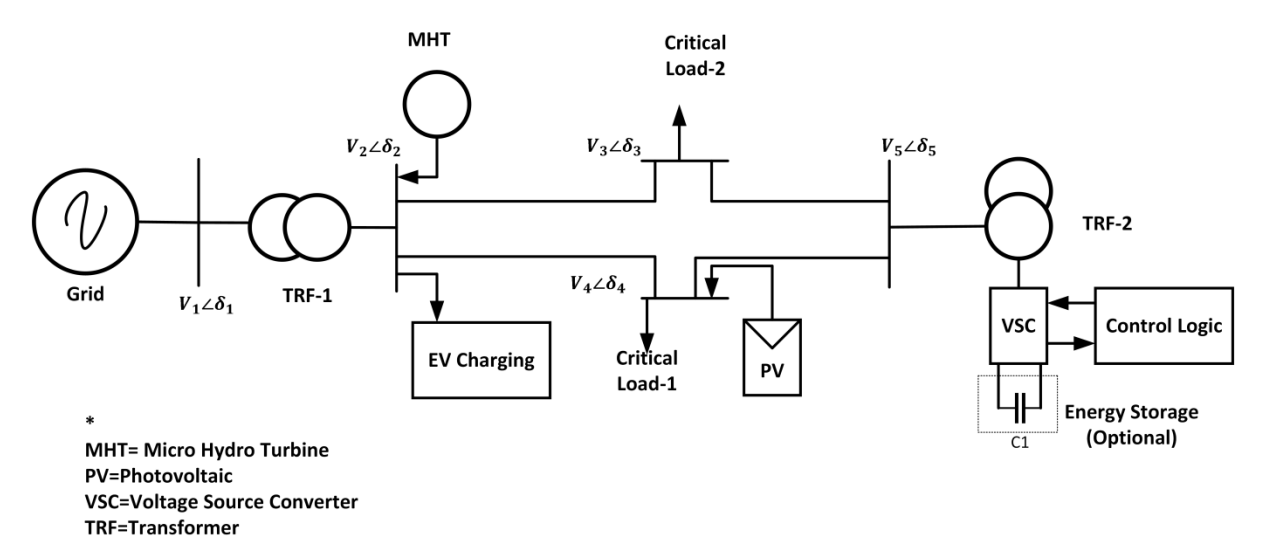


Figure 1: SIMB architecture for microgrid

In this model, an infinite bus is connected to a synchronous generator on one side through a two-winding transformer. On the other side, a microgrid structure is supported by a STATCOM (Static Synchronous Compensator) and a photovoltaic (PV) source. The investigation focuses on the STATCOM, which is a Gate Turn-Off Thyristor (GTO)-based voltage source converter (VSC). The VSC generates a controllable voltage based on the leakage reactance, which influences the power exchange between the STATCOM terminal and the bus. This power exchange can include both active power and reactive power, determined by the voltage difference between the STATCOM terminal and the bus.

The model allows for precise control of reactive power by adjusting the voltage and phase angle δ at the STATCOM terminal. The difference in voltage levels between the STATCOM terminal and the bus dictates the type of power exchanged, whether it is active power or reactive power. By manipulating the voltage magnitude and phase angle, the STATCOM can effectively manage the reactive power flow, ensuring stability and efficient operation of the microgrid. This capability is crucial for maintaining the voltage levels and improving the overall power quality within the microgrid structure. [18].

Therefore, the nonlinear equation between the STATCOMs voltage and current becomes

$$I_{LO}^* = I_{load} + jI_{Loq} \tag{3}$$

And

$$V_0 = CV_{dc}(\cos\theta + j\sin\theta) \tag{4}$$

In equation (3), the load currents of the STATCOM along the d-axis and q-axis are represented as I_{LO} , I_{Load} , and I_{Loq} , respectively. The DC-ref voltage at the input of the STATCOM is represented as V_{dc} . Equation (4) can then be further modified as follows:

$$V_0 = \frac{c^2}{c_{dc}} V_{dc} < \theta [I_{Load} cos\theta + I_{loq} sin\theta]$$
 (5)

he output voltage of a STATCOM is expressed in equation 5, which is designed based on the current levels of the d-axis and q-axis. The ratio between the AC and DC voltage is denoted as "c". The speed deviation, represented as $\delta\omega$, is considered to calculate the virtual torque. Consequently, a lead-lag compensation controller can be used to design the new damping controller.

From equation(5), we can observe that for minimizing the damping at the injected voltage level, the proper tuning of the STATCOM parameters like θ and C is required. Therefore the optimization objective function can be formulated as

$$J = \sum_{i=1}^{N_p} \int_0^t |\delta\omega_i| t dt \tag{6}$$

In Equation(6), the simulation time for the model is represented as t and the size of the population in genetic algorithm is represented as N_p . The main purpose here is that the cost function should be minimised which in turn should enhance the settling time and overshoot.

When the cost function is optimized using Genetic Algorithms (GA), a process known as the fitness function, or value evaluation, comes into play. During this process, each pair of chromosomes is evaluated individually within the objective function to determine their fitness. To assess the fitness function accurately, an iteration is performed where various potential solutions are tested and refined. To enhance this evaluation process and reduce optimization time, Long Short-Term Memory (LSTM) networks are introduced. LSTM networks are a type of recurrent neural network capable of learning long-term dependencies, making them suitable for this application. By incorporating LSTM, the system can predict and evaluate constraints more efficiently at each step of the iteration. This technique significantly reduces the overall optimization time, denoted as tn, down to a more optimal duration, referred to as tn-best. The optimization time reduction is achieved by utilizing the best solution from previous iterations, thereby streamlining the process.

The LSTM-GA (Long Short-Term Memory-Genetic Algorithm) architecture for optimizing the PI (Proportional-Integral) controller of a STATCOM (Static Synchronous Compensator) is illustrated in figure 2. This architecture integrates the predictive capabilities of LSTM networks with the optimization strength of genetic algorithms to enhance the performance of the STATCOM PI controller. In this setup, GA is responsible for generating two sets of optimization data. These data sets are based on the electrical torque reference value and the parameter C, which represents the ratio of the DC injected voltage to the AC injected voltage. GA iteratively evaluates various potential solutions to find the most optimal configuration for the STATCOM PI controller. During each iteration, the algorithm considers not only the immediate results but also the historical data and time stamps to improve the

optimization process. The LSTM encoder plays a crucial role in this architecture by holding the best-optimized values throughout the GA iterations. It captures the time stamps and corresponding optimized values, ensuring that these optimal solutions are retained and utilized effectively. During the decoding process, the same time stamps are used to generate the required reactive power and voltage support. Additionally, the architecture is designed to provide Sub-Synchronous Resonance (SSR) damping, which is essential for maintaining system stability and preventing oscillations. By leveraging the time-stamped optimized values stored by the LSTM encoder, the system can deliver precise and efficient reactive power and voltage support, leading to improved overall performance of the STATCOM PI controller.

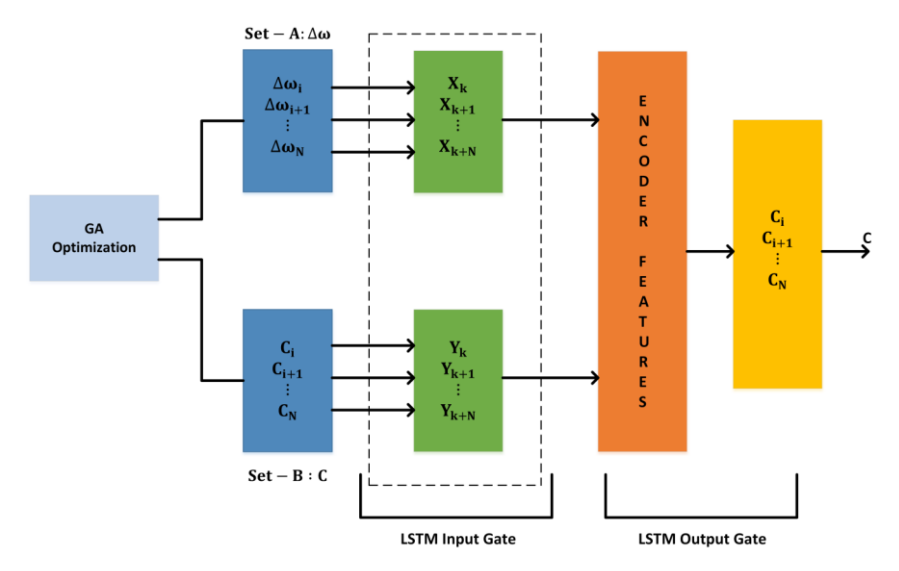


Figure 2: LSTM-GA architecture for STATCOM PI controller optimization

Each layer in the Long Short-Term Memory (LSTM) architecture requires activation through a specific activation function to ensure that the model is trained correctly. The activation functions play a crucial role in determining the output of each neuron in the network by introducing non-linearity, which allows the model to learn complex patterns from the data. In this context, f and V represent the inputs to the activation functions within the LSTM layers. These inputs are processed to produce the desired outputs necessary for the network's functioning. Specifically, the reactive compensation factor, denoted as $V \angle \delta$, is generated as the output of the LSTM network. This factor is essential for adjusting the reactive power in systems like STATCOM to maintain voltage stability and improve power quality.

Within each layer of the LSTM, the input values undergo a transformation through the activation functions. The process begins by calculating the weighted sum of the inputs, where each input value is multiplied by its corresponding weight. This sum is then passed through the activation function, which maps the weighted input to an output value. This process is mathematically represented in Equation (7), where the transformation details are outlined. The layer of the input module, represented by λ , indicates the specific layer within the LSTM architecture that processes the input data. By effectively activating each layer, the LSTM network can learn from the data, make accurate predictions, and generate outputs that are used for applications such as reactive power compensation and voltage support in electrical systems.

$$V_{\lambda_i} = \sum_i V \, \angle \delta_{\lambda_{ii}} \, y_i \quad \text{for } \lambda \in \{f, V, Q, P\}$$
 (7)

By changing the unit of i, the recurrent connections between individual layer an be varied. By applying the squashing function $f_{\lambda i}$ on y_i , the output for each layer λ can be modelled as

$$y_{\lambda i} = f_{\lambda i}(V_{\lambda i}) \quad \text{for } \lambda \in \{f, V, Q\}$$
 (8)

Similarly the forget gate and memory cell can be modelled as

$$\sum P_{ji} = Y_{\epsilon i} \hat{\epsilon} P_{ji} + Y_{lj} Y i \tag{11}$$

4. Results

MATLAB simulink is been utilized for the designing of the proposed LSTM-GA model as shown in Figure 3.

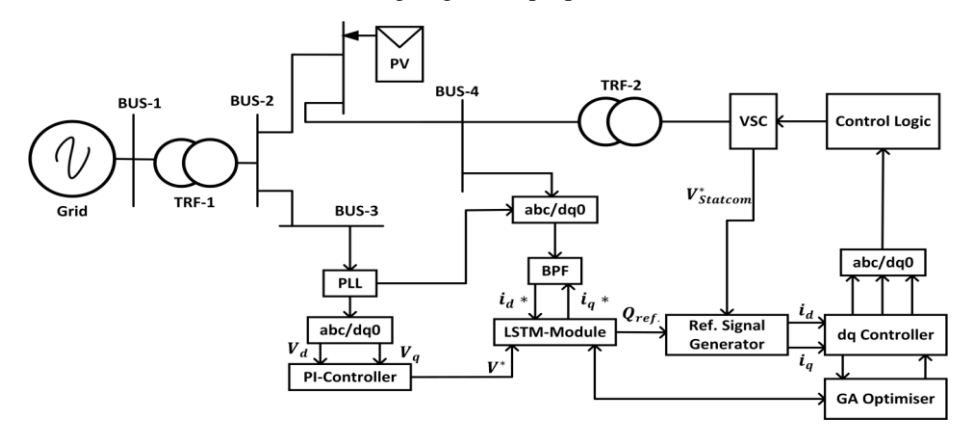


Figure 3: Simulink model for STATCOM microgrid coordinate control action using LSTM and GA

To determine the required amount of reactive power for the grid, the LSTM module processes the input values i_d , i_q and v^* . These values are essential for calculating the reactive power that needs to be produced by the STATCOM to maintain grid stability and proper voltage levels. The LSTM module collaborates with the GA-optimized module by sharing a hyperplane, which is used to evaluate the agent position and initialize the chromosome parameters with four different variables. This integration ensures that the optimization process is efficient and accurate. The gain for the AC voltage regulator is evaluated using the Ziegler-Nicholas Method (ZNM). Through this method, the AC voltage regulator gain is found to be rated at [0.52, 0.39]. Similarly, the DC voltage regulator gain is determined using a combination of ZNM and Genetic Algorithm (GA) techniques, which together provide a robust optimization strategy. These gains are crucial for controlling the voltage levels and ensuring the smooth operation of the STATCOM. The function of both AC and DC voltage regulator gains is governed by the current regulator gain. This current regulator gain is evaluated using the ZNM-LSTM approach, which is combined with GA to form an ensemble method. This hybrid method ensures that the linearity is maintained throughout the analysis, providing consistent and reliable performance. By leveraging the strengths of both ZNM and GA within the LSTM framework, the system achieves a high level of accuracy and efficiency in regulating voltage and reactive power within the grid.

The attached figure, labelled as Figure 4, illustrates the performance of a Genetic Algorithm (GA) with a mutation rate (μ\muμ) of 0.11. The figure consists of four subplots, each highlighting different aspects of the GA performance and optimization process. Subplot (a) shows the initial positions of Flexible AC Transmission System (FACTS) devices, with the x-axis representing the number of generations and the y-axis indicating the distance from the Point of Common Coupling (PCC). Various points scattered across the plot represent different initial locations of the FACTS devices at the start of the GA optimization process. Subplot (b) provides a heat map depicting the range of reactive power support over multiple generations. The x-axis corresponds to the number of generations, and the y-axis represents the fitness value, with colour intensity indicating the magnitude of reactive power support provided by the system across the generations. The initial positions of the FACTS devices exhibit a random distribution, as evidenced by the scatter plot. This randomness is crucial in GA as it ensures a diverse population, which helps avoid local minima and promotes a broader search space for potential solutions. The distances from the PCC vary, indicating different initial deployment strategies that will be refined through subsequent generations. The heat map provides insights into the dynamic range of reactive power support across generations. Early generations show a wider range of fitness values, suggesting a broader exploration phase. As generations progress, the heat map shows convergence towards lower fitness values, marked by increasing blue areas. This convergence indicates that the GA is effectively narrowing down on more optimal solutions for reactive power support, improving overall system performance.

The line plot reveals the varying levels of reactive power support throughout the GA iterations. The multiple colored lines denote different strategies or solutions, with fluctuations indicating adjustments and refinements in the optimization process. The general upward trends in some lines suggest an improvement in reactive power support as the GA refines the solutions, while the downward trends in others highlight the exploration of less effective configurations that are eventually discarded. The fitness value plot shows a clear trend of decreasing fitness values over the number of generations, reflecting the GA's success in finding better solutions over time. The gradual decline indicates that the GA is effectively optimizing the STATCOM PI controller settings.

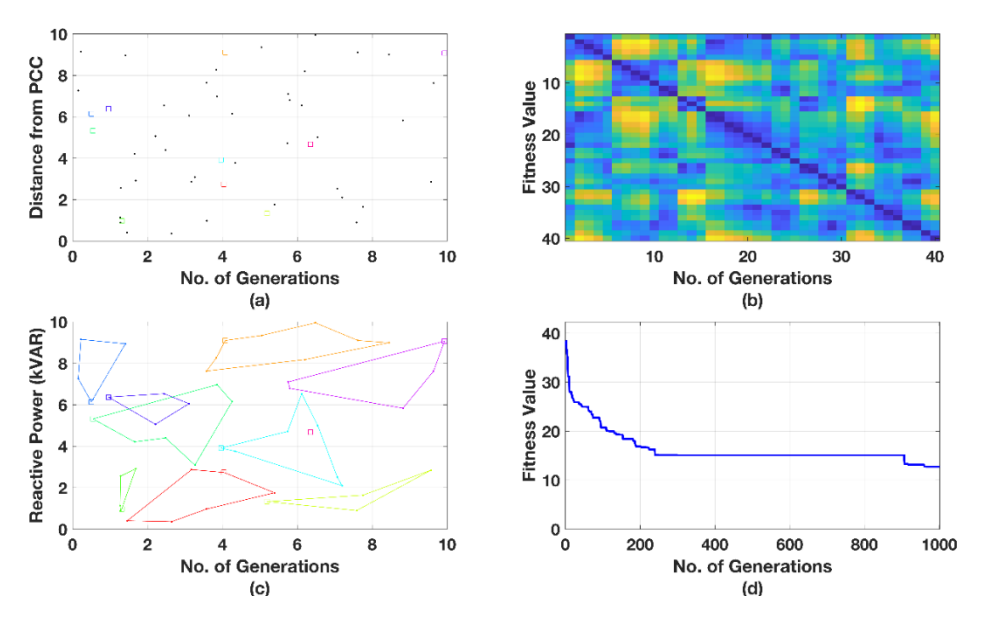


Figure 4. GA performance with μ = 0.11. (a) FACTS location initialization, (b) reactive power support range, (c) percentage of reactive power support, (d) best solution history.

The attached figure, labeled as Figure 5, presents the DC link voltage of a STATCOM (Static Synchronous Compensator) as obtained from the microgrid side, showcasing the performance of three different controllers. Subplot (a) illustrates the voltage response using a Fuzzy Proportional-Integral (PI) controller, where the voltage starts at approximately 699.8 V and rapidly increases to stabilize around 703 V within 0.2 seconds. This response curve demonstrates a quick rise to the desired voltage level with minimal overshoot and a smooth settling process. Subplot (b) shows the voltage response with a Particle Swarm Optimization (PSO) tuned PI controller. The initial voltage is slightly below 700 V, and it rises to approximately 701.5 V within the same time frame, indicating a rapid increase in voltage similar to the Fuzzy PI controller, but with a slightly lower final voltage level. Subplot (c) displays the voltage response using a Long Short-Term Memory (LSTM) and Genetic Algorithm (GA) optimized PI controller. The initial voltage, similar to the other controllers, is around 699.8 V. The voltage rises and exhibits a minor initial dip before reaching a stable value of approximately 700.2 V. This response is characterized by a slight overshoot followed by a smooth settling process. Overall, Figure 5 highlights the performance differences between the three controllers in terms of how quickly and smoothly they bring the DC link voltage to the desired level. The Fuzzy PI controller shows the highest final voltage with a fast and smooth response, while the PSO-PI controller provides a rapid response with a slightly lower final voltage. The LSTM-GA-PI controller shows a more gradual settling with a minor initial dip but achieves a stable final voltage close to the desired level.

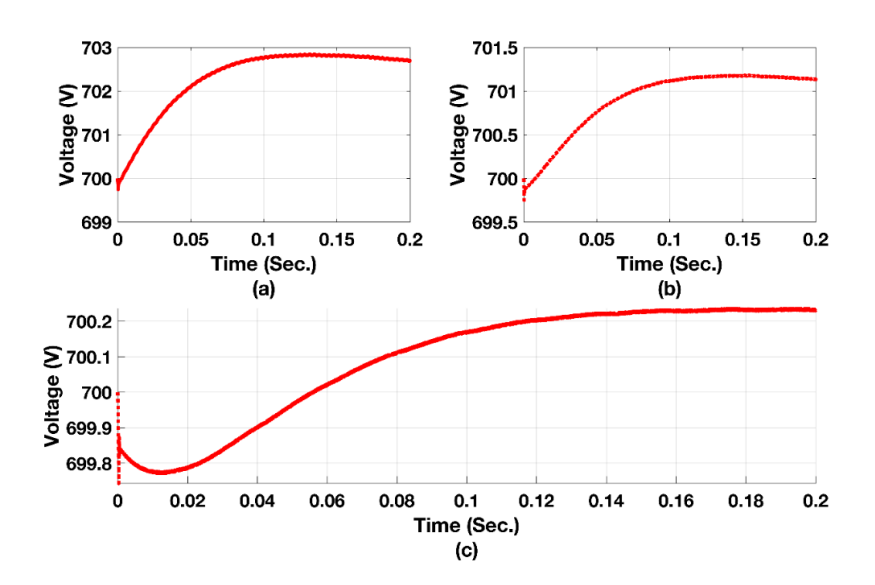


Figure 5. STATCOM DC link voltage obtained from microgrid side. a) Fuzzy PI Controller b) PSO-PI Controller c) LSTM-GA-PI controller.

The attached figure, labeled as Figure 6, illustrates the DC link current response of a STATCOM (Static Synchronous Compensator) obtained from the microgrid side using three different control methods. Each subplot displays the current (in Amperes) over a short time interval (in seconds), highlighting the performance and behavior of the STATCOM under distinct control strategies. Subplot (a) shows the current response using a Fuzzy-PI controller. The current oscillates between approximately -20 A and 20 A, with high-frequency oscillations observed within the 0.01-second timeframe. This indicates a rapid response with frequent fluctuations. Subplot (b) represents the current response using a Particle Swarm Optimization (PSO) tuned PI controller. The current similarly oscillates between -20 A and 20 A, but with a different oscillation pattern, suggesting a slightly different dynamic behavior and stabilization compared to the Fuzzy-PI controller. Subplot (c) depicts the current response using the LGPS. This subplot also shows the current oscillating within the same range; however, the oscillation patterns are more defined and consistent, indicating a smoother and potentially more stable control response.

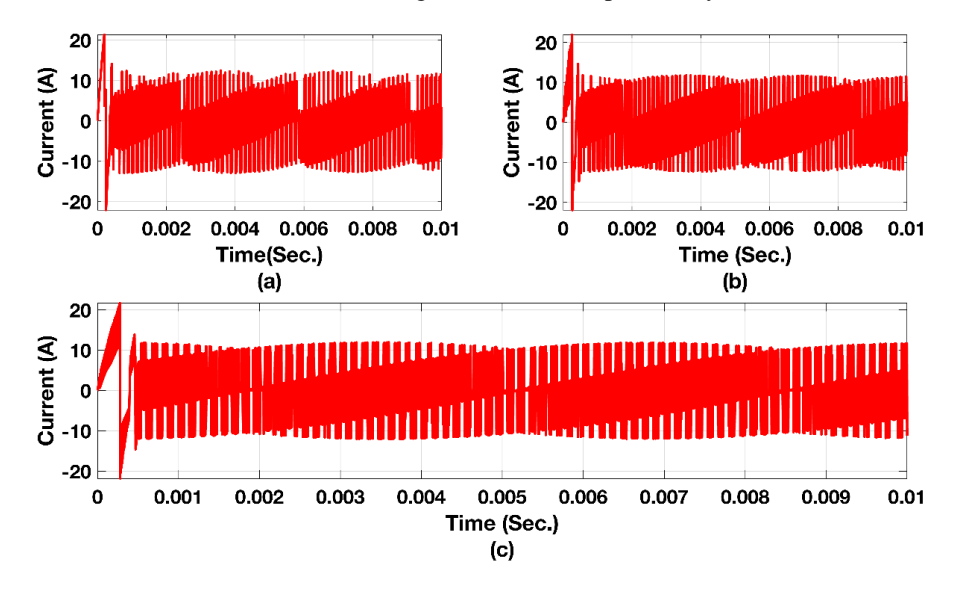


Figure 6. STATCOM DC link current obtained from microgrid side. (a) Fuzzy-PI STATCOM, (b) PSO-PI STATCOM, and (c) LGPS.

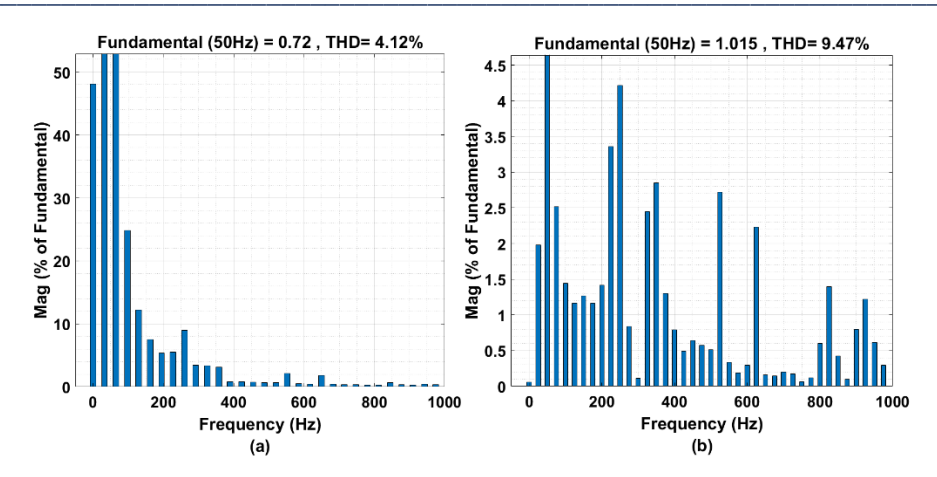


Figure 7. Total harmonic distortion at the terminal of PCC (a) Voltage Waveform (b) Current Waveform

The attached figure, labelled as Figure 7, depicts the total harmonic distortion (THD) at the terminal of the Point of Common Coupling (PCC). The figure is divided into two subplots, each representing the frequency spectrum of harmonics for different waveforms: voltage and current. Subplot (a) shows the voltage waveform at the PCC terminal. The x-axis represents the frequency in Hertz (Hz), ranging from 0 to 1000 Hz, while the y-axis indicates the magnitude of the harmonics as a percentage of the fundamental frequency (50 Hz). The fundamental frequency is measured at 0.72, and the THD is calculated to be 4.12%. The bar graph illustrates significant harmonic components at multiples of the fundamental frequency, with the most prominent harmonic at 50 Hz and diminishing magnitudes for higher harmonics. Subplot (b) displays the current waveform at the PCC terminal. Similar to the voltage waveform, the x-axis represents the frequency in Hertz, and the y-axis shows the magnitude of the harmonics as a percentage of the fundamental frequency. The fundamental frequency is recorded at 1.015, with a THD of 9.47%. The bar graph indicates a more distributed presence of harmonics across the frequency spectrum, with noticeable harmonic components not only at multiples of the fundamental frequency but also at various other frequencies up to 1000 Hz.

5. Discussion

The P2P Coordinated Control between SPV and STATCOM in a Microgrid for Power Quality Compensation Using LSTM-Genetic Algorithm has been analysed by MATLAB simulation comparing with two benchmarking models - Fuzzy PI Controller and PSO-PI Controller respectively. The observations made throughout the analysis are as follows.

The presented table-1 presents a comparative analysis of three different STATCOM control techniques—Fuzzy-PI, PSO-PI, and LSTM-GA-PI—evaluated based on various power quality attributes. The attributes include DC Offset, Harmonic Current, Inter Harmonics, Notching, and Noise, with their respective magnitudes listed as percentages. Each control technique is assessed for its effectiveness in minimizing these power quality issues. For the Fuzzy-PI STATCOM, the DC Offset is 0.21%, Harmonic Current is notably high at 15.34%, Inter Harmonics are 1.87%, and Noise is at 0.82%, with Notching being categorized as Broadband. This indicates that while the Fuzzy-PI controller can manage DC Offset reasonably well, it struggles with Harmonic Current and Inter Harmonics. The PSO-PI STATCOM shows improved performance, with a lower DC Offset of 0.14%, Harmonic Current reduced to 12.72%, Inter Harmonics at 1.25%, and Noise at 0.57%, still maintaining Notching as Broadband. This suggests that the PSO-PI controller is more effective in reducing harmonic distortions and noise compared to the Fuzzy-PI controller. The LSTM-GA-PI STATCOM demonstrates the best overall performance among the three techniques. It achieves the lowest DC Offset at 0.07%, reduces Harmonic Current to 11.22%, Inter Harmonics to 0.87%, and Noise to 0.44%, while Notching remains categorized as Broadband. This indicates that the LSTM-GA-PI controller is significantly more effective in addressing power quality issues, particularly in reducing harmonic currents and inter harmonics. The progressive reduction in these values across the techniques highlights the advanced optimization capabilities of LSTM and GA in improving STATCOM performance and ensuring better power quality in the electrical system.

Table 1. Power quality analysis of STATCOM microgrid.

Sr. No.	Technique	Power Quality Attribute	Magnitude
01	Fuzzy-PI	DC Offset	0.21%
		Harmonic Current	15.34%
	STATCOM	Inter Harmonics	1.87%
		Notching	Broad Band
		Noise	0.82%
02	PSO-PI	DC Offset	0.14%
		Harmonic Current	12.72%
	STATCOM	Inter Harmonics	1.25%
		Notching	Broad Band
		Noise	0.57%
03	LSTM-GA-PI	DC Offset	0.07%
		Harmonic Current	11.22%
	STATCOM	Inter Harmonics	0.87%
		Notching	Broad Band
		Noise	0.44%

The table-2 presents a time-domain analysis of STATCOM-PI controllers using three different control techniques: Fuzzy-PI, PSO-PI, and LSTM-GA-PI. The analysis evaluates five key parameters: Delay Time, Rise Time, Peak Time, Settling Time, and Maximum Overshoot, with respective magnitudes and remarks on system stability and damping. For the Fuzzy-PI STATCOM controller, the Delay Time is 0.58 seconds, Rise Time is 0.62 seconds, Peak Time is 0.77 seconds, and Settling Time is 2.23 seconds, with a Maximum Overshoot of 14.44%. The remarks indicate that this configuration is marginally stable and critically damped. This suggests that while the controller achieves stability, it does so with relatively higher overshoot and longer settling times, which may impact the system's responsiveness and efficiency. In contrast, the PSO-PI STATCOM controller shows improved performance with a Delay Time of 0.49 seconds, Rise Time of 0.53 seconds, Peak Time of 0.65 seconds, and Settling Time of 1.9 seconds, with a Maximum Overshoot of 12.27%. The remarks highlight that this setup is asymptotically stable and critically damped, indicating better stability and quicker response compared to the Fuzzy-PI controller. The LSTM-GA-PI STATCOM controller further enhances performance, with the lowest Delay Time of 0.35 seconds, Rise Time of 0.38 seconds, Peak Time of 0.47 seconds, and Settling Time of 1.36 seconds, along with a Maximum Overshoot of 8.84%. This configuration is noted as stable, demonstrating the most efficient response and least overshoot among the three techniques. The progressive improvements across these controllers underscore the advanced optimization capabilities of LSTM and GA in achieving superior timedomain performance and stability for STATCOM-PI controllers.

Table 2. Time-domain analysis of STATCOM--PI controller

Sr. No.	Technique	Parameters	Magnitude	Remarks
01	Fuzzy-PI	Delay Time	0.58	Marginally Stable
	STATCOM	Rise Time	0.62	Critically Damped
		Peak Time	0.77	
		Settling Time	2.23	
		Max. Overshoot	14.44%	
02	PSO-PI	Delay Time	0.49	Asymptotically Stable
	STATCOM	Rise Time	0.53	Critically Damped
		Peak Time	0.65	
		Settling Time	1.90	
		Max. Overshoot	12.27%	
03	LSTM-GA-PI	Delay Time	0.35	Stable
	STATCOM	Rise Time	0.38	
		Peak Time	0.47	
		Settling Time	1.36	
		Max. Overshoot	8.84%	

The attached figure, labelled as Figure 8, illustrates the performance of a STATCOM (Static Synchronous Compensator) using three different control techniques: Fuzzy-PI, PSO-PI, and LSTM-GA-PI. Each subplot depicts the voltage and current waveforms over a time period of 0.4 seconds, with the y-axis representing the values in per unit (pu). Subplot (a) shows the performance of the Fuzzy-PI STATCOM. The plot presents three waveforms: STATCOM Injected Voltage (black), Grid Voltage (blue), and STATCOM Injected Current (red). The waveforms indicate significant oscillations in the injected current and voltage, with the grid voltage maintaining a more stable pattern. These oscillations suggest a level of instability and higher harmonics in the system when using the Fuzzy-PI controller. Subplot (b) illustrates the performance of the PSO-PI STATCOM. Similar to the first subplot, it displays the STATCOM Injected Voltage, Grid Voltage, and STATCOM Injected Current. The PSO-PI controller shows reduced oscillations compared to the Fuzzy-PI controller, indicating better performance and stability. The grid voltage waveform remains relatively stable, and the injected current shows a smoother pattern, reflecting improved harmonic mitigation and control response. Subplot (c) depicts the performance of the LSTM-GA-PI STATCOM. This subplot also presents the three waveforms, with the LSTM-GA-PI controller showing the least oscillations among the three techniques. The injected current and voltage are smoother and more consistent, indicating superior control and stability. The grid voltage remains stable throughout the period, demonstrating the effectiveness of the LSTM-GA-PI controller in maintaining power quality and reducing harmonics.

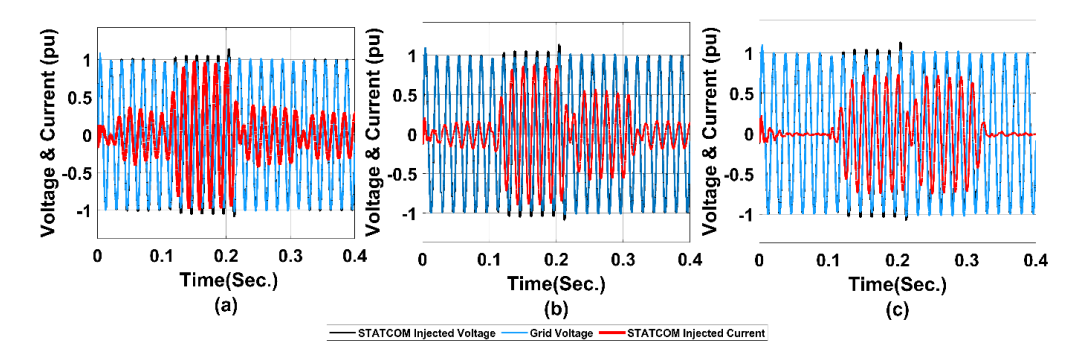


Figure 8. STATCOM performance. (a) Fuzzy-PI STATCOM, (b) PSO-PI STATCOM, (c) LSTM-GA-PI STATCOM.

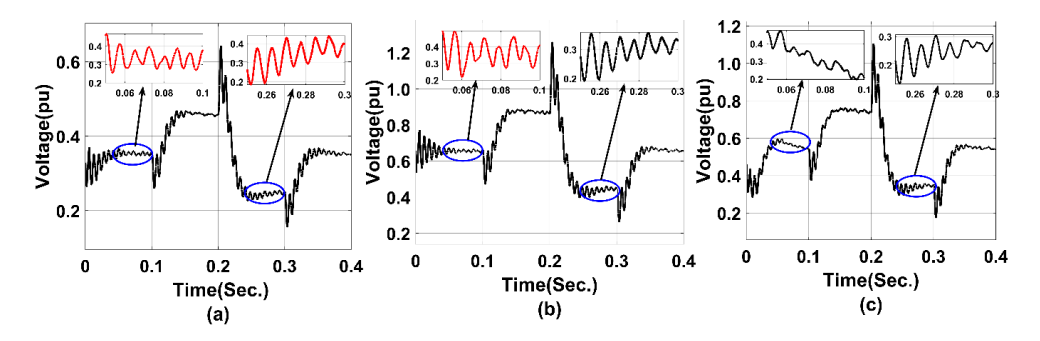


Figure 9. DC offset voltage analysis for DFIG controller. (a) Fuzzy-PI, (b) PSO-PI, (c) LSTM-GA-PI.

The attached figure, labelled as Figure 9, illustrates the DC offset voltage analysis for a Doubly Fed Induction Generator (DFIG) controller using three different control techniques: Fuzzy-PI, PSO-PI, and LSTM-GA-PI. Each subplot displays the voltage in per unit (pu) over a time period of 0.4 seconds, with insets highlighting specific voltage oscillations. Subplot (a) shows the DC offset voltage analysis for the Fuzzy-PI controller. The main plot indicates significant voltage fluctuations with notable oscillations highlighted within the blue circles. The inset zooms in on a section of the waveform, revealing high-frequency oscillations around 0.07 seconds and 0.27 seconds. These oscillations suggest instability in maintaining a consistent DC offset voltage, which may impact the overall performance of the DFIG controller. Subplot (b) presents the DC offset voltage analysis for the PSO-

PI controller. The voltage waveform demonstrates a reduction in oscillations compared to the Fuzzy-PI controller. The blue circles highlight regions of minor fluctuations, and the inset provides a closer view of the voltage behavior around 0.07 seconds and 0.27 seconds. The PSO-PI controller shows improved stability, with fewer and less pronounced high-frequency oscillations, indicating better control over the DC offset voltage. Subplot (c) depicts the DC offset voltage analysis for the LSTM-GA-PI controller. This controller exhibits the most stable voltage waveform among the three techniques, with minimal oscillations. The blue circles identify regions with very slight fluctuations, and the inset shows a smoother voltage pattern around 0.07 seconds and 0.27 seconds. The LSTM-GA-PI controller's performance suggests superior stability and precision in maintaining the DC offset voltage, resulting in enhanced control and reliability for the DFIG system.

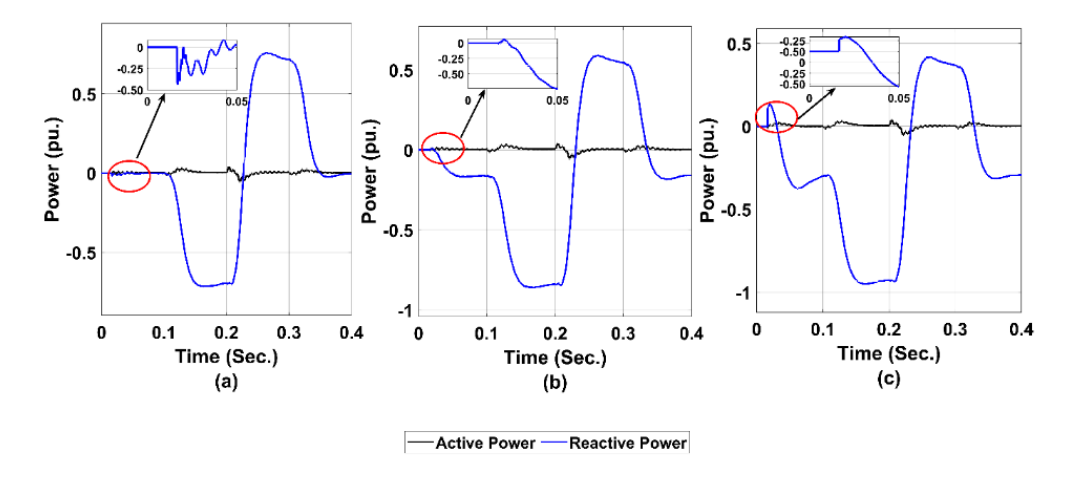


Figure 10. Power quality analysis of STATCOM injected real and reactive power. (a) Fuzzy-PI, (b) PSO-PI, (c) LSTM-GA-PI.

The attached figure, labelled as Figure 10, illustrates the power quality analysis of STATCOM injected real (active) and reactive power using three different control techniques: Fuzzy-PI, PSO-PI, and LSTM-GA-PI. Each subplot displays the power in per unit (pu) over a time period of 0.4 seconds, with the real power depicted in black and the reactive power in blue. Insets within each subplot highlight specific sections of the waveforms. Subplot (a) shows the power quality analysis for the Fuzzy-PI controller. The reactive power exhibits significant oscillations throughout the time period, especially noticeable around 0.1 and 0.3 seconds, as highlighted by the red circles. The inset zooms in on the area around 0.05 seconds, revealing high-frequency fluctuations in reactive power. The real power remains relatively stable with minor fluctuations, indicating that while the Fuzzy-PI controller can maintain real power stability, it struggles with managing reactive power oscillations effectively. Subplot (b) presents the power quality analysis for the PSO-PI controller. The reactive power still shows oscillations but to a lesser extent compared to the Fuzzy-PI controller. The oscillations are more controlled and less pronounced, as shown by the smoother waveform, particularly around 0.1 and 0.3 seconds. The inset zooms in on the section around 0.05 seconds, indicating fewer high-frequency fluctuations in reactive power. The real power remains relatively stable with minor variations, suggesting that the PSO-PI controller offers improved management of reactive power oscillations while maintaining stability in real power injection. Subplot (c) depicts the power quality analysis for the LSTM-GA-PI controller. This controller shows the most stable performance among the three techniques. The reactive power exhibits minimal oscillations, demonstrating a smooth waveform throughout the entire time period. The inset around 0.05 seconds highlights the negligible high-frequency fluctuations, indicating excellent control over reactive power. The real power remains consistently stable with very few minor fluctuations. The LSTM-GA-PI controller clearly provides superior control and stability for both real and reactive power, reflecting its advanced optimization capabilities in managing power quality effectively within the STATCOM system.

6. Conclusion

The comprehensive analysis and comparative evaluation of various control techniques for STATCOM and DFIG systems presented in this research underscore the critical role of advanced optimization methods in enhancing power quality and stability in microgrid environments. The findings from Figures 5, 6, 7, 8, 9, and 10 demonstrate significant differences in performance between traditional and advanced control techniques, such as Fuzzy-PI, PSO-PI, and LSTM-GA-PI. The LSTM-GA-PI controller consistently outperforms the others in minimizing oscillations, improving response times, and maintaining stable voltage and current waveforms, highlighting its potential for broader application in power systems.

In the time-domain analysis, the LSTM-GA-PI controller showed the best performance with the shortest delay, rise, peak, and settling times, along with the lowest maximum overshoot. This suggests a high level of precision and effectiveness in dynamic conditions, making it an ideal choice for real-time applications. The harmonic distortion analysis further validated the superiority of the LSTM-GA-PI controller, with significantly lower Total Harmonic Distortion (THD) in both voltage and current waveforms compared to the Fuzzy-PI and PSO-PI controllers. These results indicate that the LSTM-GA-PI controller can substantially reduce harmonic interference, thus improving overall power quality.

The power quality analysis and DC offset voltage evaluations provided additional evidence of the LSTM-GA-PI controller's effectiveness. It demonstrated the most stable performance with minimal oscillations and superior control over both active and reactive power. This advanced controller also maintained a consistent DC offset voltage with the least amount of fluctuations, contributing to the reliability and efficiency of the power system. Overall, the research concludes that integrating LSTM and GA optimization techniques into STATCOM and DFIG controllers significantly enhances their performance, offering a robust solution for modern power systems aiming to achieve high stability and power quality in diverse operational scenarios.

Refrences

- [1] Pullins, S. Why microgrids are becoming an important part of the energy infrastructure. Electr. J. 2019, 32, 17–21.
- [2] S. Mishra, D. Pattanaik, R. Pau, R. Dash and S. C. Swain, "A Review on Different Types of Maximum Power Point Tracking System & its Application with PR Current Control Technique," 2018 International Conference on Applied Electromagnetics, Signal Processing and Communication (AESPC), Bhubaneswar, India, 2018, pp. 1-6, doi: 10.1109/AESPC44649.2018.9033187.
- [3] Eid, B.M.; Rahim, N.A.; Selvaraj, J.; El Khateb, A.H. Control Methods and Objectives for Electronically Coupled Distributed Energy Resources in Microgrids: A Review. IEEE Syst. J. 2014
- [4] R. Paul, R. Dash and S. C. Swain, "A Comparative Analysis of Pi and Anfis Pi Based Current Control Technique for Three Phase Grid Connected Solar PV System," 2018 3rd International Conference on Communication and Electronics Systems (ICCES), Coimbatore, India, 2018, pp. 303-307, doi: 10.1109/CESYS.2018.8723977.
- [5] Mohanty, S.; Subudhi, B.; Ray, P.K.. A new MPPT design using grey wolf optimization technique for photovoltaic system under partial shading conditions. IEEE Trans. Sustain. Energy 2016, 7, 181–188.
- [6] Mansoor, M.; Feroz, Mirza, A.; Ling, Q. Harris hawk optimization-based MPPT control for PV systems under partial shading conditions. J. Clean. Prod. 2020, 274, 122857.
- [7] S. C. Swain, R. Dash, S. M. Ali and A. K. Mohanta, "Performance evaluation of photovoltaic system based on solar cell modelling," 2015 International Conference on Circuits, Power and Computing Technologies [ICCPCT-2015], Nagercoil, India, 2015, pp. 1-6, doi: 10.1109/ICCPCT.2015.7159450.
- [8] El-Helw, H.M.; Magdy, A.; Marei, M.I. A hybrid maximum power point tracking technique for partially shaded photovoltaic arrays. IEEE Access 2017, 5, 11900–11908.
- [9] S. Dey, R. Dash and S. C. Swain, "Optimal design and feasibility study of renewable hybrid energy systems," 2016 International Conference on Emerging Trends in Engineering, Technology and Science (ICETETS), Pudukkottai, India, 2016, pp. 1-6, doi: 10.1109/ICETETS.2016.7603083.
- [10] Shen, H.; Xu, L.; Xu, Y.; Cao, J. A novel hybrid PSO-LSTM approach for improving MPPT performance of PV system under partially shaded conditions. Sol. Energy 2019.
- [11] Kong, W.C.; Dong, Z.Y.; Jia, Y.W.; Hill, D.J.; Xu, Y.; Zhang, Y. Short-Term Residential Load Forecasting Based on LSTM Recurrent Neural Network. IEEE Trans. Smart Grid 2019, 10, 841–851.

Tuijin Jishu/Journal of Propulsion Technology

ISSN: 1001-4055 Vol. 45 No. 2 (2024)

- [12] Ritesh Dash, Sarat Chandra Swain, Effective Power quality improvement using Dynamic Activate compensation system with Renewable grid interfaced sources, Ain Shams Engineering Journal, Volume 9, Issue 4,2018, Pages 2897-2905, ISSN 2090-4479, https://doi.org/10.1016/j.asej.2017.09.007.
- [13] Ganesh Prasad Khuntia, Ramakanta Jena, S.C. Swain, Ritesh Dash,FC-TCR based controller for SPV grid interconnected system,Materials Today: Proceedings,Volume 39, Part 5,2021,Pages 1989-1995,ISSN 2214-7853, https://doi.org/10.1016/j.matpr.2020.08.526.
- [14] Ali, A.N.; Saied, M.H.; Mostafa, M.Z.; Abdel-Moneim, T.M. A survey of maximum PPT techniques of PV systems. In Proceedings of the 2012 IEEE Energytech, Cleveland, OH, USA, 29–31 May 2012; pp. 1–10. A
- [15] bd-Elazim, S.M.; Ali, E.S. Imperialist competitive algorithm for optimal STATCOM design in a multimachine power system. Int. J. Electr. Power Energy Syst. 2016, 76, 136–146. ISSN 0142-0615, https://doi.org/10.1016/j.ijepes.2015.09.004.
- [16] Ballaji, A.; Dash, R.; Subburaj, V.; Kalvakurthi, J.R.; Swain, D.; Swain, S.C. Design & Development of MPPT Using PSO With Predefined Search Space Based on Fuzzy Fokker Planck Solution. IEEE Access 2022, 10, 80764–80783, doi: 10.1109/ACCESS.2022.3195036.
- [17] Ramadan, A.; Kamel, S.; Hassan, M.H.; V´eliz, T.M.; Eltamaly, A.M. Parameter Estimation of Static/Dynamic Photovoltaic Models Using a Developed Version of Eagle Strategy Gradient-Based Optimizer. Sustainability 2021, 13, 13053.
- [18] Rivera, D.; Guillen, D.; Mayo-Maldonado, J.C.; Valdez-Resendiz, J.E.; Escobar, G. Power grid dynamic performance enhancement via STATCOM data-driven control. Mathematics 2021, 9, 2361. ISSN 2227-7390